Dalton Transactions

Cite this: *Dalton Trans.*, 2011, **40**, 11866

www.rsc.org/dalton

PAPER

Self assembled tetranuclear Cu_4(II), Ni_4(II) [2 × 2] square grids and a dicopper(II) complex of heterocycle based polytopic ligands - Magnetic studies†‡

Tarak Nath Mandal,[a] Somnath Roy,[a] Saugata Konar,[a] Atanu Jana,[a] Sangita Ray,[a] Kinsuk Das,[a] Rajat Saha,[b] Mohamed Salah El Fallah,*[c] Ray J. Butcher,[d] Sudipta Chatterjee[e] and Susanta Kumar Kar*[a]

Received 2nd May 2011, Accepted 23rd August 2011
DOI: 10.1039/c1dt10813a

The ditopic ligand PyPzOAP (*N*-[(*Z*)-amino(pyridin-2-yl)methylidene]-5-methyl-1-(pyridin-2-yl)-1*H*-pyrazole-3-carbohydrazonic acid) and the polytopic ligand 2-PzCAP (N'^3,N'^5-bis[(1*E*)-1-(pyridin-2-yl)-ethylidene]-1*H*-pyrazole-3,5-dicarbohydrazide) were synthesized *in situ* by condensation of methyl imino picolinate with 5-methyl-1-(2-pyridyl) pyrazole-3-carbohydrazide and 2-acetyl pyridine with pyrazole-3,5-dicarbohydrazide respectively. The ligands PyPzOAP and PzOAP (reported earlier, *Dalton Trans.*, 2007, 1229) self-assemble to form homoleptic [2 × 2] tetranuclear M_4 (M = Cu(II) and Ni(II)) square grids structures $[Cu_4(PyPzOAP)_4](NO_3)_4$ (**1**), $[Cu_4(PzOAP)_4](ClO_4)_4$ (**2**) and $[Ni_4(PyPzOAP)_4](NO_3)_4{\cdot}8H_2O{\cdot}2CH_3CN$ (**3**). While the ligand 2-PzCAP forms a dicopper(II) complex $[Cu_2(2\text{-}PzCAP)(OH)(NO_3)(H_2O)](NO_3){\cdot}2H_2O$ (**4**). The complex **1** is a perfect square grid (a = 4.201 Å), whereas, **2** and **3** are almost square grids. All these compounds have been characterized by X-ray structural analyses and variable temperature magnetic susceptibility measurements. EPR studies have also been carried out for complexes **1**, **2** and **4**. In the Cu_4 grid (**1**), all the Cu(II) centers are in a distorted octahedral environment with N_4O_2 chromophore, while, in complex **2**, all four Cu(II) centers have a square pyramidal environment with N_3O_2 chromophore. In complex **3**, all four Ni(II) centers have distorted octahedral geometry with N_4O_2 chromophore. In compound **4**, the Cu(II) centers are in square pyramidal environment with N_3O_2 chromophore. The magnetic properties of compounds **1** and **2** show the presence of intramolecular ferromagnetic exchange interaction (J = 5.88 cm^{-1} for **1** and 4.78 cm^{-1} for **2**). The complex **3** shows weak intramolecular antiferromagnetic interaction (J = –4.02 cm^{-1}). While, complex **4**, shows strong antiferromagnetic behavior (J = –443 cm^{-1}).

Introduction

The binding of transition metal ions to properly designed polytopic ligands has attracted continuous scientific interest since the seminal reports on the metal-mediated self-assembly processes.[1–3] Self-assembly of transition metals with multifunctional organic ligands represent a successful paradigm for the single step synthesis of new clusters of well-defined aesthetical architectures with electronic, redox, magnetic, photo-physical and catalytic properties.[4–7] The major challenging goal in this area is the design and synthesis of new polytopic ligands which can be used for synthesis of molecular metal grids. Hence, with the proper choice of paramagnetic metal ions which interact with these polytopic ligands, magnetic coupling can be fine-tuned. Spin exchange interactions occur between the paramagnetic metal ions through the direct bridging (*e.g.* μ-O, μ-N–N) connections of the ligands.[8] Moreover, depending on the packing, such assemblages have the unique potential to exhibit either long-range order or single molecule magnetic behavior. Transition metal ion templated cyclizations have successfully produced many tetranuclear [2 × 2] Mn_4, Ni_4, Cu_4 and Zn_4 grid complexes,[9–15] in which the bridging arrays among the metal ions involve oxygen donor groups. Most of the so far reported alkoxo-bridged polynuclear grids [Mn(II), Co(II) and Ni(II)][11–15] show anti-ferromagnetic coupling, while the ferromagnetic interaction prevails only in Cu(II) grids.[8b–d,16] The origin of this ferromagnetic exchange is due to the orthogonal

[a]*Department of Chemistry, University College of Science, University of Calcutta, 92, A.P.C. Road, Kolkata, 700 009, India. E-mail: skkar_cu@yahoo.co.in*
[b]*Department of Physics, Jadavpur University, Kolkata, 700 032, India*
[c]*Departament de Química Inorgànica, and Institut de Nanociència i Nanotecnologia, Universitat de Barcelona, Martí i Franquès 1-11, 08028, Barcelona, Spain. E-mail: salah.elfallah@qi.ub.es*
[d]*Department of Chemistry, Howard University, 2400 Sixth Street, N.W., Washington, DC, 200 59, USA*
[e]*Department of Chemistry, Serampore College, Serampore, Hooghly, Pin - 712 201, India*

† Electronic supplementary information (ESI) available. CCDC reference numbers 796246–796249 for **1**–**4**. For ESI and crystallographic data in CIF or other electronic format see DOI: 10.1039/c1dt10813a

‡ Dedicated to the late Dr Golam Mostafa.

orientation of the magnetic orbitals ($d_{x^2-y^2}$). Thus, the major direction in the syntheses of new magnetically coupled metal grids and clusters is the exploration of the various super-exchange bridges embedded inside the polytopic ligands which will lead to the development of materials with the desired magnetic properties.

In this work, we have continued our pursuit of studying the coordination properties of N-heterocycle-based polytopic ligands. As a part of this effort, we herein report two such new ligands, PyPzOAP and 2-PzCAP (Scheme 1). The ligand PyPzOAP formed a ferromagnetically coupled Cu_4(II) [2 × 2] square grid (**1**) and a weak antiferromagnetically coupled Ni_4(II) [2 × 2] square grid (**3**). While, PzOAP formed a ferromagnetically coupled Cu_4(II) [2 × 2] square grid (**2**). A polytopic ligand 2-PzCAP (1 : 2 condensation product of pyrazole-3,5-dicarbohydrazide and 2-acetyl pyridine) formed only a dicopper(II) complex (**4**) instead of a molecular grid. All the complexes are structurally and magnetically characterized. EPR studies have also been carried out for complexes **1**, **2** and **4**.

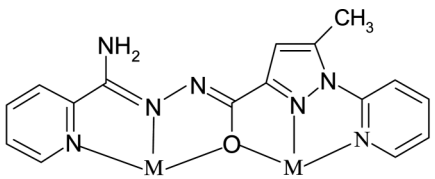

PyPzOAP

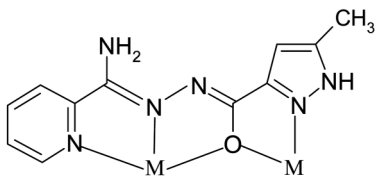

PzOAP

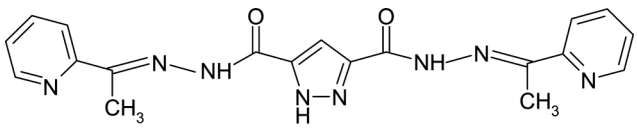

2-PzCAP

Scheme 1

Experimental

Materials

2-Cyano pyridine, 2-cyanopyrazine and 2-acetyl pyridine were purchased from Aldrich. Other commercially available chemicals and solvents were used and purified by standard procedures.[17]

Caution! Although we have not encountered any problem, it should be kept in mind that only a small amounts of perchlorate compound should be prepared and it should be handled with care.

Physical measurement

Elemental analyses (carbon, hydrogen and nitrogen) of the ligand and the metal complexes were determined with a Perkin-Elmer CHN analyzer 2400. Mass spectra were done with a JEOLJMS-AX 500 mass spectrometer. The electronic spectra of the complexes were recorded on a Hitachi model U-3501 spectrophotometer. IR spectra (KBr pellet, 400–4000 cm^{-1}) were recorded on a Perkin-Elmer model 883 infrared spectrophotometer. Magnetic susceptibility measurements for the compounds were carried out on polycrystalline samples, at the Servei de Magnetoquímica of the Universitat de Barcelona, with a Quantum Design SQUID MPMS-XL susceptometer apparatus working in the range 2–300 K under a magnetic field of approximately 500 G (2–30 K) and 1000 G (35–300 K). Diamagnetic corrections were estimated from Pascal Tables. The EPR spectra have been recorded on an X-band Bruker spectrometer (ESR 300E) working with an Oxford helium liquid cryostat for variable temperature measurements.

Syntheses of the ligands

5-methyl-1-(2-pyridyl)pyrazole-3-carbohydrazide was prepared following our previously reported method.[18] The ligand PzOAP was synthesized as reported previously.[8b,c] Pyrazole-3,5-dicarbohydrazide was prepared according to the literature procedure.[19]

Synthesis of PyPzOAP

The methyl ester of iminopicolinic acid was prepared *in situ* by reaction of 2-cyanopyridine (5.2 g, 0.05 mol) with sodium methoxide solution, produced by dissolving sodium metal (2.5 g, 0.108 mol) in dry methanol (25 mL). 5-methyl-1-(2-pyridyl) pyrazole-3-carbohydrazide (10.85 g, 0.05 mol) in 25–30 mL dry methanol, was added to the above solution with stirring for 1 h. The mixture was refluxed for 5 h and cooled to room temperature. Excess methanol was removed in a rotary evaporator to leave a yellow coloured oily sticky liquid. It was then mixed with water (50 mL) and neutralized with AcOH (pH~5) which afforded a shining yellow powder. The solid was filtered off, washed thoroughly with water and methanol and dried *in vacuo* over fused $CaCl_2$. Yield (10.43 g, 65%). Mp 220 °C (decomp.). MS (*m*/*z*) 321 (M^+, 100%). IR/cm^{-1}: ν_{NH} 3360; $\nu_{CO/CN}$ 1655(s), 1540(s); ν_{N-Npz} 1060(s); ν_{py} 1006(s). Anal. calc. for $C_{16}H_{15}N_7O$: C, 59.81; H, 4.67; N, 30.52. Found: C, 59.40; H, 4.62; N, 30.60%.

Synthesis of 2-PzCAP

To a dry methanolic solution (30 mL) of 2-acetyl pyridine (0.242 g, 2 mmol), solid pyrazole-3,5-dicarbohydrazide (0.184 g, 1 mmol) was added with constant stirring. The suspension was stirred for 30 min and refluxed for 5 h at water bath temperature. After reflux, the suspension turned into a transparent solution. The volume of the mixture was reduced to one-third of its original volume and kept for slow evaporation. After two days, a white microcrystalline solid product was afforded. The solid was filtered off, washed several times with cold methanol and dried *in vacuo* over fused $CaCl_2$. Yield: 0.341 g, 80%. M.P. 197–200 °C (decomp.). MS (*m*/*z*) 390 (M^+, 100%). IR/cm^{-1}: ν_{NH} 3348; $\nu_{CO/CN}$ 1673(s), 1536(s); ν_{N-Npz} 1123(s); ν_{py} 1005(s). Anal. calc. for $C_{19}H_{18}N_8O_2$: C, 58.46; H, 4.61; N, 28.72. Found: C, 58.55; H, 4.65; N, 28.69%.

Table 1 Crystallographic data of **1–4**

Compound	**1**	**2**	**3**	**4**
Empirical formula	$C_{64}H_{56}Cu_4N_{32}O_{16}$	$C_{44}H_{44}Cl_4Cu_4N_{24}O_{20}$	$C_{68}H_{75}Ni_4N_{34}O_{24}$	$C_{19}H_{24}Cu_2N_{10}O_{12}$
Formula weight	1783.61	1625.04	1987.29	711.56
T/K	293 (2)	150(2)	293(2)	200(2)
Wavelength (Å)	0.71073	0.71073	0.71073	0.71073
Crystal system	Monoclinic	Monoclinic	Tetragonal	Triclinic
Space group	$C2/c$	$P2_1/c$	$I4_1/a$	$P\bar{1}$
Unit cell dimensions	a = 19.921(7) Å b = 38.224(16) Å c = 14.084(5) Å $\alpha = \gamma = 90°$ β = 134.890(5)	a = 14.745(1) Å b = 21.597(1) Å c = 26.180(2) Å $\alpha = \gamma = 90°$, β = 121.57(1)°	a = 14.105(9) Å b = 14.105(9) Å c = 38.379(4) Å $\alpha = \beta = \gamma = 90°$	a = 8.8162(4) Å b = 10.2990(5) Å c = 16.3062(5) Å α = 74.779(3)° β = 88.629(3)° γ = 65.135(4)°
Volume (Å^3)	7598(5)	7103.1(11)	7636(7)	1289.87(9)
Z	4	2	4	2
Density (calc) (Mg m^{-3})	1.559	1.520	1.719	1.832
Absorption Coefficient (mm^{-1})	1.192	1.413	1.076	1.733
F(000)	3632	3280	4056	724
θ Range (°) for data collection	1.07 to 20.41	4.69 to 32.48	1.54 to 24.07	4.55 to 34.78
Index ranges	$-19 \le h \le 19$ $-37 \le k \le 37$ $-13 \le l \le 13$	$-21 \le h \le 21$ $-31 \le k \le 30$ $-38 \le l \le 37$	$-16 \le h \le 16$ $-16 \le k \le 16$ $-44 \le l \le 44$	$-13 \le h \le 14$ $-15 \le k \le 16$ $-21 \le l \le 25$
Goodness-of-fit on F^2	1.190	1.043	1.086	0.965
Completeness to θ	99.6%(= 20.00°)	98% (= 32.48°)	99.7% (24.07°)	99.2% (34.78°)
Independent reflections [R_{int}]	3741 [0.0305]	25170 [0.0572]	3019 [0.0382]	10328 [0.0224]
Refinement method	Full-matrix least squares on F^2	Full-matrix least squares on F^2	Full-matrix least squares on F^2	Full-matrix least squares on F^2
Data/restraints/parameters	3741/0/523	25170/0/869	3019/0/285	10328/46/454
Reflections collected	22805	58450	41211	22018
Final R indices [$I > 2\sigma(I)$]	R_1 = 0.0619, wR_2 = 0.1122	R_1 = 0.0992, wR_2 = 0.2698	R_1 = 0.0535, wR_2 = 0.1256	R_1 = 0.0345, wR_2 = 0.0832
R indices (all data)	R_1 = 0.0776, wR_2 = 0.1178	R_1 = 0.1792, wR_2 = 0.3486	R_1 = 0.0572, wR_2 = 0.1284	R_1 = 0.0591, wR_2 = 0.0875
Largest difference peak and hole (e Å^{-3})	0.255 and –0.213	2.289 and –0.905	1.351and –0.488	1.103 and –0.852

Syntheses of the complexes

$[Cu_4(PyPzOAP)_4](NO_3)_4$ (1). The ligand PyPzOAP (0.321 g, 1 mmol) was added to a hot solution of $Cu(NO_3)_2{\cdot}6H_2O$ (0.148 g, 1 mmol) in H_2O/CH_3OH (30 mL) [60 : 40 v/v]. The resulting suspension was stirred with heating (~60 °C) until complete dissolution of the ligand occurred. The resulting deep green solution was filtered to remove any undissolved ligand and left at room temperature. Dark green crystals suitable for X-ray diffraction were isolated from the filtrate after standing for two weeks. Yield 0.211 g, 45%. IR/cm^{-1}: ν_{NH} 3372; $\nu_{CO/CN}$ 1665(s), 1535(s); ν_{N-Npz} 1060(s); ν_{py} 1020(s). UV-vis (λ_{max}): 670 nm. μ_{RT} 3.67 B.M. Anal. calc. for $C_{64}H_{56}Cu_4N_{32}O_{16}$: C, 43.05; H, 3.13; N, 25.11. Found: C, 43.10; H, 3.18; N, 25.15%.

$[Cu_4(PzOAP)_4](ClO_4)_4$ (2). Complex **2** was prepared following the same procedure as that of complex **1** using $Cu(ClO_4)_2{\cdot}6H_2O$ as metal salt. Yield 0.429 g, 70%. IR/cm^{-1}: ν_{NH} 3350, 3134; $\nu_{CO/CN}$ 1645(s), 1525(s); ν_{N-Npz} 1051(s); ν_{py} 1021(s). UV-vis (λ_{max}): 368, 694(br)nm. μ_{RT} 3.54 B.M. Anal. calc. for $C_{44}H_{44}Cl_4Cu_4N_{24}O_{20}$: C, 32.49; H, 2.70; N, 20.68. Found: C, 32.53; H, 2.72; N, 20.55%.

$[Ni_4(PyPzOAP)_4](NO_3)_4{\cdot}8H_2O{\cdot}2CH_3CN$ (3). The ligand PyPzOAP (0.321 g, 1 mmol) was added to a hot solution of $Ni(NO_3)_2{\cdot}6H_2O$ (0.29 g, 1 mmol) taken in H_2O/CH_3CN (20 mL) [60 : 40 v/v]. Then pH of the solution was adjusted to *ca.* 6 by adding few drops of NEt_3. A red coloured compound precipitated and the stirring was continued for *ca.* 45 min. This was filtered under suction, washed with methanol and dried over fused $CaCl_2$. X-ray quality crystals of **3** were obtained by slow evaporation of acetonitrile solution of the complex. Yield 0.245 g, 40%. IR/cm^{-1}: ν_{NH} 3365; $\nu_{CO/CN}$ 1660(s), 1532(s); ν_{N-Npz} 1056(s); ν_{py} 1030(s). UV-vis (λ_{max}): 392, 630, 990 nm. μ_{RT} 6.11 B.M. Anal. calc. for $C_{68}H_{75}Ni_4N_{34}O_{24}$: C, 41.06; H, 3.77; N, 23.95. Found: C, 41.04; H, 3.74; N, 23.91%.

$[Cu_2(2\text{-}PzCAP)(OH)(NO_3)(H_2O)](NO_3){\cdot}2H_2O$ (4). The ligand 2-PzCAP (0.195 g, 0.5 mmol) was added to a solution of $Cu(NO_3)_2{\cdot}6H_2O$ (0.295 g, 1 mmol) in CH_3CN-H_2O (30 mL) [10 : 1 v/v]. The suspension was stirred for 1 h with constant stirring at ~60 °C until complete dissolution of the ligand occurred. The resulting deep green solution was filtered and left at room temperature. Rectangular dark green crystals suitable for X-ray diffraction were isolated after standing for several days. Yield: 0.270 g, 55%. IR/cm^{-1}: $\nu_{NH/H2O}$ 3372, 3136; $\nu_{CO/CN}$ 1669(s), 1533(s); ν_{N-Npz} 1119(s); ν_{py} 997(s). UV-vis (λ_{max}): 385, 590(br) nm. μ_{RT} 1.85 B.M. Anal. calc. for $C_{19}H_{24}Cu_2N_{10}O_{12}$: C, 32.06; H, 3.37; N, 19.67. Found: C, 32.10; H, 3.39; N, 19.65%.

Single crystal X-ray crystallography

Selected crystal data for **1–4** are given in Table 1 and selected metrical parameters of these complexes are given in Table 2. For **1** and **3** the data collections were made using Bruker SMART APEX II CCD area detector equipped with graphite monochromated Mo-Kα radiation (λ = 0.71073 Å) source in ω scan mode. For **2** and **4**, data collections were made using Oxford Diffraction

Table 2 Selected bond distances (Å) and angles (°) in **1–4**

Selected bonds	Value (Å)	Selected angles (°)	
Complex 1			
Cu1–O1	2.376(5)	N4–Cu1–N2A	175.7(3)
Cu1–N4	1.895(7)	N4–Cu1–O2	99.2(2)
Cu1–N6	2.329(8)	N2A–Cu1–O2	77.2(3)
Cu1–O2	2.064(5)	N4–Cu1–N1A	105.7(3)
Cu1–N1A	2.086(7)	N2A–Cu1–N1A	78.0(4)
Cu1–N2A	1.983(7)	O2–Cu1–N1A	154.7(3)
Cu2–N4A	1.913(7)	N4–Cu1– N6	72.0(4)
Cu2– N2	1.998(8)	N2A–Cu1–N6	105.5(3)
Cu2– O1	2.070(5)	O2–Cu1–N6	92.2(2)
Cu2– N1	2.070(7)	N1A–Cu1–N6	99.2(2)
Cu2– N6A	2.348(8)	N4–Cu1–O1	74.0(3)
Cu2– O2	2.388(5)	O2–Cu1–O1	91.83(18)
		N4A–Cu2–N2	175.9(3)
		N4A–Cu2–O1	99.1(2)
		N2–Cu2–O1	77.5(3)
		O1–Cu2–N1	155.3(3)
		O1–Cu2–N6A	90.9(2)
		N2–Cu2–O2	108.3(2)
		O1–Cu2–O2	92.01(18)
Complex 2			
Cu1–O1	1.958(5)	Cu1–O4–Cu4	136.4(4)
Cu1–O4	2.333(4)	Cu1–O1–Cu2	139.0(2)
Cu1–N1	2.050(7)	Cu2–O2–Cu3	138.2(2)
Cu1–N3	1.903(5)	Cu3–O3–Cu4	138.3(2)
Cu1–N23	1.961(5)	O1–Cu1–N3	79.7(2)
Cu2–O1	2.324(6)	N3–Cu1–N23	167.7(2)
Cu2–O2	1.967(4)	O1–Cu1–N1	159.6(2)
Cu2–N5	1.952(5)	O1–Cu2–N5	76.2(2)
Cu2–N7	1.994(6)	N5–Cu2–N9	168.2(3)
Cu2–N9	1.915(7)	O1–Cu2–N5	76.2(2)
Cu2–O2	2.396(6)	N11–Cu3–N15	176.1(3)
Cu3–O3	1.985(5)	O3–Cu3–N13	159.5(2)
Cu3–N11	1.969(5)	N13–Cu3–O2	95.1(3)
Cu3–N13	2.030(7)	N17–Cu4–N21	173.36(19)
Cu3–N15	1.887(5)	O4–Cu4–N19	159.8(3)
Cu3–O3	2.302(4)	O4–Cu4–N17	97.2(2)
Cu4–O4	1.958(5)	N17–Cu4–N19	102.4(3)
Cu4–N17	1.983(5)	N19–Cu4–N21	81.0(3)
Cu4–N19	2.020(7)		
Cu4–N21	1.926(6)		
Complex 3			
Ni1–O1	2.079(3)	O1–Ni1–N1	154.78(12)
Ni1–N1	2.115(3)	O1–Ni1–N2	77.46(11)
Ni1–N2	1.958(4)	O1–Ni1–O1^b	92.31(10)
Ni1–O1^b	2.280(3)	O1–Ni1–N4^b	105.68(11)
Ni1–N4^b	1.936(3)	O1–Ni1–N6^b	94.08(11)
Ni1–N6^b	2.177(3)	N1–Ni1–N2	77.38(13)
		O1^b–Ni1–N1	91.46(10)
		N1–Ni1–N4^b	99.23(13)
		N1–Ni1–N6^b	96.33(11)
		O1^b–Ni1–N2	102.85(11)
		N2–Ni1–N4^b	174.17(12)
		N2–Ni1–N6^b	110.34(13)
		O1^b–Ni1–N4^b	72.33(11)
		O1^b–Ni1–N6^b	146.80(12)
		N4^b–Ni1–N6^b	74.58(13)
		Ni1–O1–Ni1^a	137.83(13)
Complex 4			
Cu1–O	1.9197(11)	O–Cu1–N4A	88.91(5)
Cu1–N4A	1.9289(13)	O–Cu1–N1A	99.14(5)
Cu1–N1A	1.9590(14	N4A–Cu1–N1A	169.25(6)
Cu1–N2A	2.0251(13)	O–Cu1–N2A	169.48(6)
Cu1–O11A	2.264(7)	N4A–Cu1–N2A	89.32(5)
Cu1–O11B	2.38(3)	N1A–Cu1–N2A	81.47(6)
Cu2–O	1.9142(11)	O–Cu1–O11A	90.59(12)
Cu2–N4B	1.9201(13)	O–Cu2–N4B	89.32(5)
Cu2–N1B	1.9622(13)	O–Cu2–N1B	98.88(5)
Cu2–N2B	2.0154(13)	N4B–Cu2–N1B	169.02(6)
		O–Cu2–N2B	177.46(5)
		N4B–Cu2–N2B	89.71(5)
		N1B–Cu2–N2B	81.79(5)
		Cu2–O–Cu1	118.43(6)
		Cu2–O–H1O	113.3(16)
		Cu1–O–H1O	111.7(16)

Complex **3**:^{a} Symmetry elements = 5/4 $-y$,$-3/4+x$,1/4 $-z$, ^{b} Symmetry elements = 3/4+y,5/4 $-x$,1/4 $-z$.

Gemini and Oxford Diffraction Gemini R equipped with graphite monochromated Mo-Kα radiation (λ = 0.71073 Å) source φ–ω scan mode. For **1** and **3** the structures were solved using the Patterson method by using the SHELXS-97.[20] Subsequent difference Fourier synthesis and least-square refinement revealed the positions of the remaining non hydrogen atoms. Non-hydrogen atoms were refined with independent anisotropic displacement parameters. Hydrogen atoms were placed in idealized positions and their displacement parameters were fixed to be 1.2 times larger than those of the attached non-hydrogen atom. Successful convergence was indicated by the maximum shift/error of 0.001 for the last cycle of the least squares refinement. All calculations were carried out using SHELXS-97,[20] SHELXL-97,[20] PLATON-99,[21] ORTEP-32[22] and WinGX system Ver-1.64.[23] For **2** and **4**, cell parameter refinement and data reduction were carried out using the CRYSALIS RED, Oxford Diffraction Ltd., Version 1.171.31.8 (release 12-01-2007 CRYSALIS171. NET) and Version 1.171.32.15 (release 10-01-2008 CRYSALIS171. NET) respectively. All the structures were solved by conventional direct methods and refined by full-matrix least square methods using F^2 data. SHELXS-97 and SHELXL-97 programs[20] were used for structure solution and refinement respectively. For **3**, H-atoms were not included in acetonitrile and water molecules. For complex **1**, due to the wrong data collection strategy the data are complete only to θ = 20° resulting in a low data : parameter ratio and, in consequence, in a low-bond precision. Thus it would not be appropriate to use these bond parameters in fine comparison with similar entities in future. Since we failed to generate another suitable quality single crystal of this compound it thus restricts the possibility to recollect the data to rectify this problem. But it suffices to establish the identity, connectivity of the molecule and gross feature of the system. We have critically examined the data and found that R_2 value is higher for the 'Tetragonal' system than that in the 'Monoclinic' system. In the Tetragonal system the R_2 value is 0.218 whereas in the Monoclinic system the R_2 value is 0.031. The structure can be solved both in Tetragonal as well as Monoclinic systems and the structural model is the same. The reported structure model exhibits a partial pseudosymmetry. Thus we decided to solve it in the 'Monoclinic' crystal system. Compound **2** appears to be crystalline but, in general, was not suitable for X-ray study. Fortunately, after several trials X-ray quality crystals of $[Cu_4(PzOAP)_4](ClO_4)_4$ could be formed. Crystals of this compound were found to be weak scatterers and thus the quality of the structure is not very high. However, the structural analysis of the reference compound suffices to establish the identity and gross features of the system.

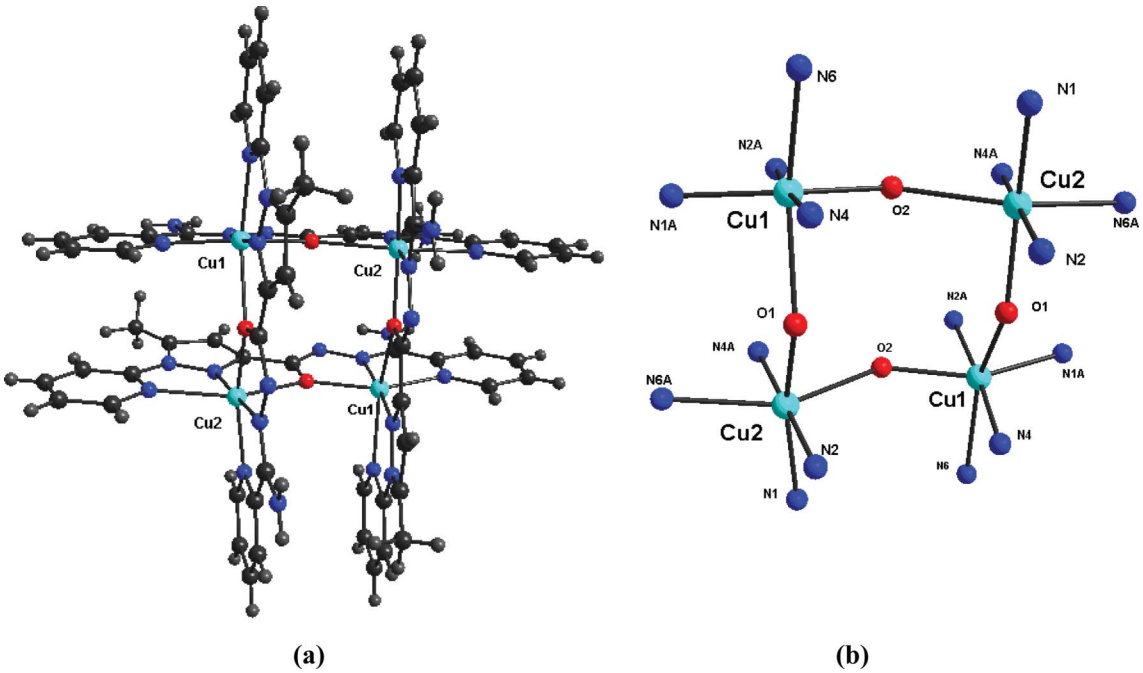

Fig. 1 (a) Structural representation of cationic complex **1**. (b) Structural representation with atom numbering scheme of the tetranuclear core in **1**.

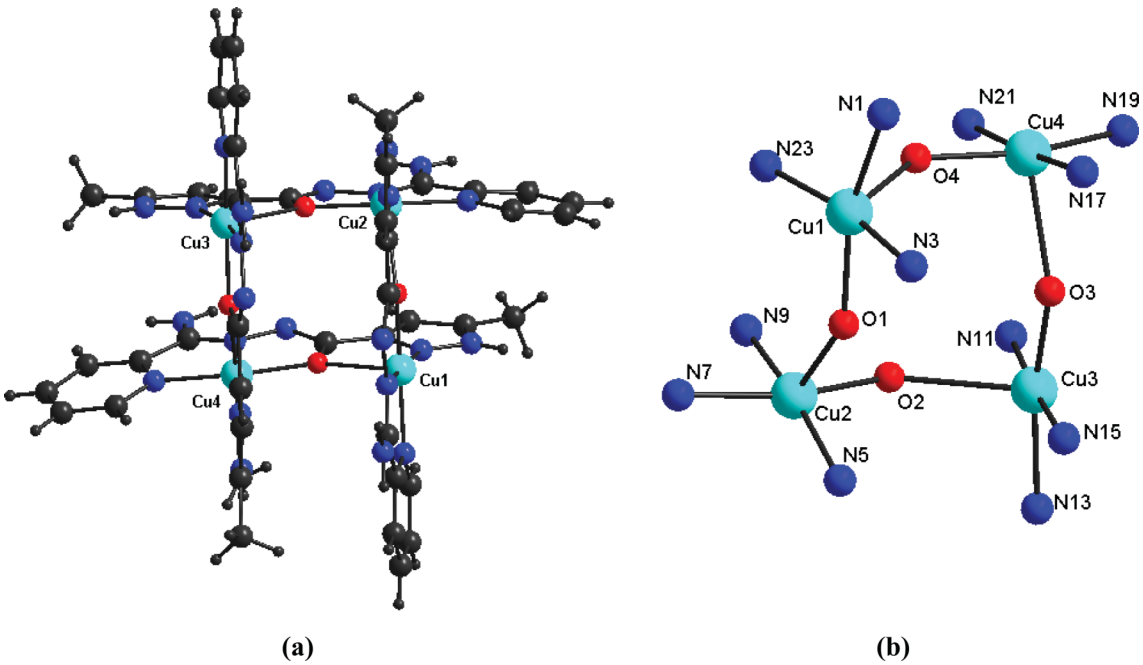

Fig. 2 (a) Structural representation of cationic complex **2**. (b) Structural representation with atom numbering scheme of the tetranuclear core in **2**.

Results and discussion

Structural description of 1, 2 and 3

The structures of the tetranuclear cationic part in **1–3** are illustrated in Fig. 1(a), 2(a) and 3(a) respectively. The core structures are shown in Fig. 1(b), 2(b) and 3(b) respectively. The complex **1** is a homoleptic Cu_4(II) [2 × 2] square grid, where all four Cu(II) centers are bridged by alkoxide oxygen atoms. It consists of four six-coordinate distorted octahedra with N_4O_2 chromophore where all the copper(II) centers are arranged in a perfect square (a = 4.199 Å), with alkoxide oxygen atoms acting as connector between the two adjacent metal atoms. The alkoxide bridge angles are in the range 141.0(3)–141.6(3)°. For this complex, the ligands PyPzOAP are aligned in two parallel pairs, above and below the tetra copper square arrangements. The two-fold rotational symmetry leads to two equivalent pairs of copper centers with an alternating arrangement of axial [Cu1–O1 2.376(5) Å, Cu2–O2 2.388(5) Å] and equatorial Cu–O bonds [Cu1–O2 2.064(5) Å, Cu2–O1 2.070(5) Å] around the square. The Jahn–Teller axis

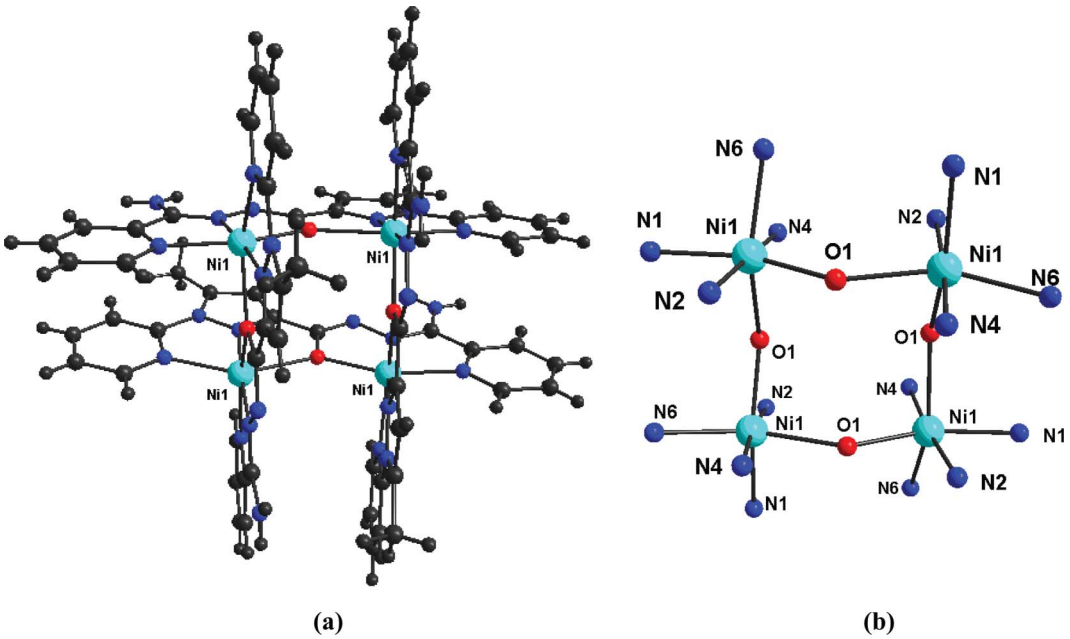

Fig. 3 (a) Structural representation of cationic complex **3**. (b) Structural representation with atom numbering scheme of the tetranuclear core in **3**.

of Cu1 and Cu2 are defined as O1–Cu1–N6 (Cu1–O1 2.376(5) Å, Cu1–N6 2.329(8) Å) and O2–Cu2–N6A (Cu2–O2 2.388(5) Å, Cu2–N6A 2.348(8) Å), with the equatorial planes O2–N2A–N1A–N4 and O1–N2–N1–N4A respectively.

For complex **2**, all the four copper(II) centers are arranged in a squarish manner. The ligands (PzOAP) are arranged in two parallel pairs, above and below the tetra copper square arrangements. The Cu–Cu separations are closed to 4 Å (Cu1–Cu2 4.014 Å, Cu2–Cu3 4.079 Å, Cu3–Cu4 4.008 Å and Cu4–Cu1 3.987 Å) with O–Cu–O bridge angles falling in the range 94.97(17)–96.37(16)°. Here all the square pyramidal Cu1, Cu2, Cu3 and Cu4 centers have the CuN_3O_2 chromophore. The structure of **2** involves the use of the four five-coordinate Cu(II) centers for formation of the homoleptic Cu_4 [2 × 2] square grid.

Complex **3** consists of a [2 × 2] square grid involving four nickel(II) centers bridged by four alkoxide oxygen atoms. Here the PyPzOAP ligand behaves as a uninegative-pentadentate N_4O donor, where the oxygen atom acts as a bridging atom between the two adjacent nickel(II) centers. Each nickel atom has distorted octahedral geometry and is bound to two pyridine nitrogen atoms, one pyrazole nitrogen atom, one imine nitrogen atom, and two alkoxide oxygen atoms belonging to two orthogonal ligands. All the Ni–Ni bond lengths are exactly 4.067 Å forming a perfect Ni_4 [2 × 2] square grid. All the Ni–O bonds have alternating long and short distances (2.280(3) and 2.079(3) Å respectively) around the Ni_4O_4 arrangement. All the Ni–O–Ni angles are 137.83(13)°. Two of the oxygen atoms are located above the mean Ni_4 plane (0.765 Å), while the other two are located below it (0.765 Å) resulting a boatlike arrangement. Each of the Ni(II) atom have four short in-plane bonds (1.936(3)–2.115(3) Å), formed by the three nitrogen atoms (N1, N2 and N4) and one oxygen atom of ligand moiety in the equatorial plane. While the apical positions are occupied by one nitrogen atom (N6) and one oxygen atom with longer distance (Ni1–O1 2.280(3) Å and Ni1–N6 2.177(3) Å). The shorter Ni–N6 bond distance than that of Ni–O1 suggests that the central Ni(II) atom is slightly pulled toward the N6 atom (mean plane deviation, 0.068 Å) from the basal plane formed by the equatorial atoms. From the analysis of all nickel–nitrogen/oxygen bond distances it is clear that each nickel environment undergoes tetragonal elongation. The pyridyl-pyrazole part of the ligand PyPzOAP is planar (dihedral angle 1.44°) as that of complex **1**. All the three complexes are stabilized through H-bond networks. In the case of **1**, there is moderately strong H-bonding involving the hydrogen atoms of dangling -NH_2 groups with the oxygen atoms of ionic nitrate. In **2** there are weak H-bonding interactions involving hydrogen atoms of pyrazole-N and dangling -NH_2 group with the oxygen atoms of ionic perchlorate. Relevant H-bond parameters are listed in the ESI (Table-S1†). In **3** weak H-bonding exist between H2W1 of water molecule and N3 atom of ligand moiety, H7A and H7B of free –NH_2 group and O1 W of water and O101 of nitrate molecule respectively. The nitrate anions present in this molecule is responsible for the formation honeycomb like superstructure (Fig. 4). This is a unique example of a honeycomb network consisting of a self-assembly of Ni_4(II) grid.

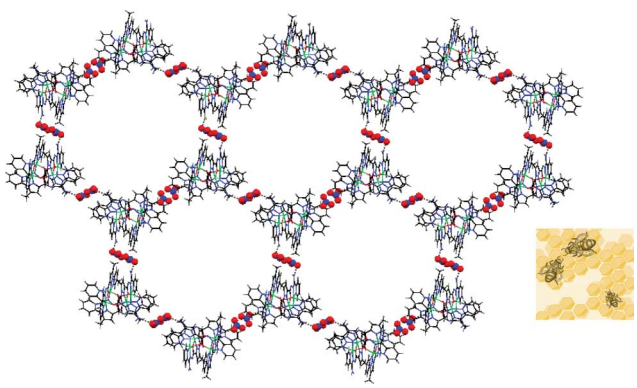

Fig. 4 Honeycomb like superstructure of **3** (Solvent molecules were omitted for clarity).

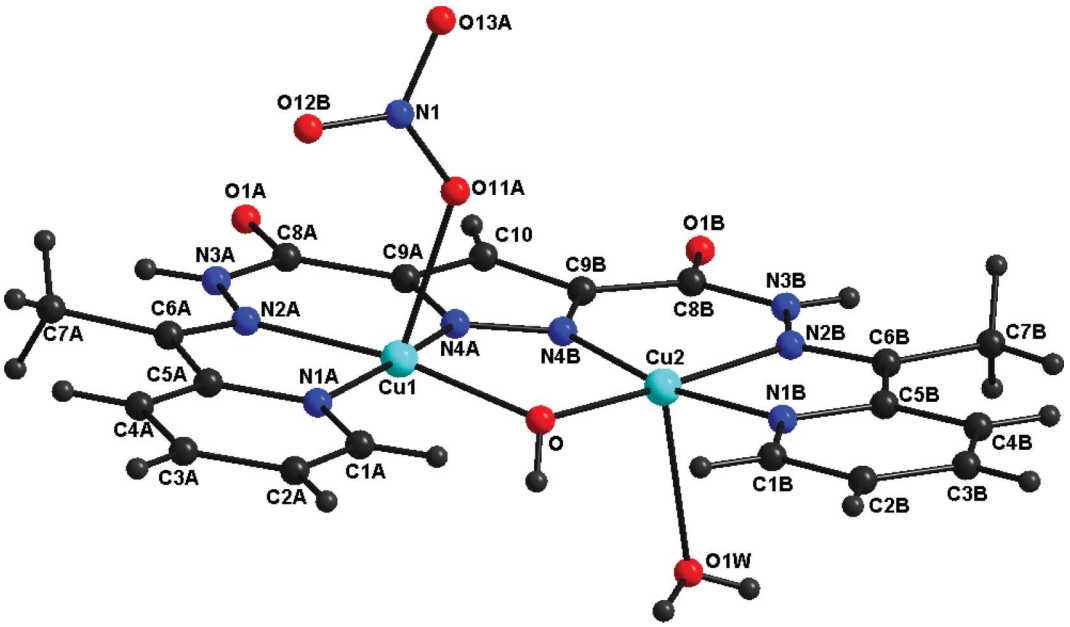

Fig. 5 Structural representation and atom numbering scheme of the cationic complex **4**.

Structural description of 4

The structural representation of **4** is shown in Fig. 5. The structure consists of a dinuclear cation, with two copper centers bridged by the central pyrazole moiety and an adventitious hydroxide group. The ligand adopts an unusual *cis* conformation, in which the hydrazone oxygen and diazine N–N groups are not involved in bridging and the ligand end pieces form a tridentate N3 coordinating pocket, with a mixture of five- and six-membered chelate rings. The net result is a near perfect fit of the metal ions in the pockets forming an almost planar dinuclear entity. The Cu–Cu separation is 3.294 Å and the Cu–O–Cu angle is 118.43(6)°. The two copper ions are almost square pyramidal (τ values are 0.004 for Cu1 and 0.14 for Cu2), with an axial nitrate bound to Cu1 and an axial water molecule bound to Cu2 forming an unusual *trans* arrangements between them. Hence, the absence of any intramolecular hydrogen bonding interaction indicates the inherent stability of the dinuclear unit and the apparently preferred dinucleating ligand bonding mode. In this complex, there is a weak H-bonding interaction involving H3AB and H3BB with O3W and O2W respectively of lattice water molecules. Details of H-bond parameters are provided in the ESI (Table-S1†).

Magnetic studies

The variable temperature magnetic susceptibility data for the compounds **1** and **2** in form $\chi_M T$ *vs* T plots is shown in Fig. 6 indicating ferromagnetic behaviors of the two compounds. $\chi_M T$ values are 1.672 $cm^3\ mol^{-1}$ K (for **1**) and 1.556 $cm^3 mol^{-1}$ K (for **2**) at 300 K being close to that expected for four uncoupled $S = 1/2$ spins (with $g = 2.1$ for **1** and 2.00 for **2**). $\chi_M T$ increases up slightly when temperature was lowered and reached a maximum value of 3.162 $cm^3\ mol^{-1}$ K and 2.878 $cm^3\ mol^{-1}$ K at 2 K for **1** and **2** respectively. These maxima are consistent with that expected for a ferromagnetically coupled copper(II) ions.

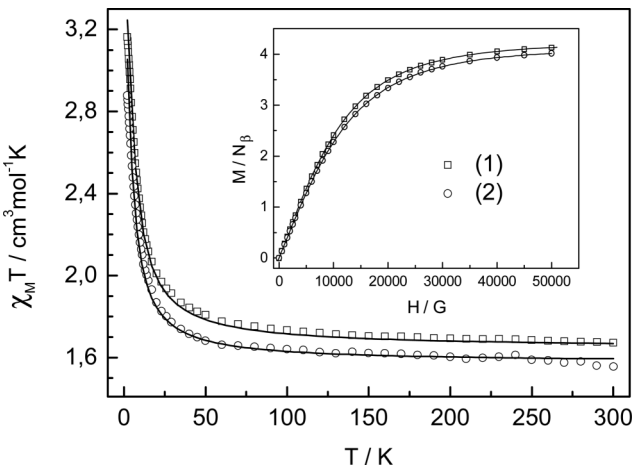

Fig. 6 Plots of the $\chi_M T$ *vs* T and $M\ N^{-1}\beta$ *vs* H at $T = 2$ K (inset) for **1** and **2**. Solid line corresponds to the best fit (see text). The experimental magnetization curves of the complexes (**1**) and (**2**) were fitted to the Brillouin equation at $T = 2.0$ and $S = 2.0$ giving the following values of $g = 2.08$ for **1** and $g = 2.02$ for **2**.

The field dependence of magnetization (0–5 T) measured at 2 K of **1** and **2** shown in Fig. 6, inset in the form of $M\ N^{-1}\beta$ (per Cu4 entity) *vs* H suggests that the magnetization tends to 4 Nβ. This feature agrees with the global weak ferromagnetic coupling within the four copper(II) atoms.

The structures of **1** and **2** consist of copper ions linked between them by the ligands PyPzOAP and PzOAP giving tetranuclear compounds respectively. Taking into account the compound topology (slight distortion from square array, see crystallographic data), coupling parameters J, (Fig. 7) can be considered to interpret the magnetic interactions in the complex. For this square disposition, the E_n value can be obtained by using Kambe method[24] from the Hamiltonian:

$$H = -J_1(S_1 \cdot S_2 + S_2 \cdot S_3 + S_3 \cdot S_4 + S_1 \cdot S_4) \quad (1)$$

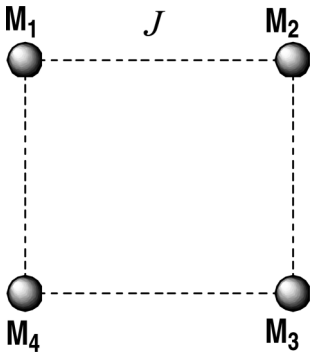

Fig. 7 Structural representation of the $[M_4O_4]$ core and exchange coupling constant in **1**, **2** and **3**. (M = Cu in **1** and **2**, and M = Ni in **3**).

The analysis of the experimental susceptibility data have been performed by the use of expression:

$$\chi_M = \frac{Ng^2\beta^2}{3K}\frac{6\exp(J/KT)+12\exp(2J/KT)+30\exp(3J/KT)}{1+3\exp(J/KT)+7\exp(2J/KT)+5\exp(3J/KT)} \quad (2)$$

The parameters N, β and K in eqn (2) have their usual meanings, J = Singlet–triplet splitting.

The best fit parameters found are: $J = +5.88$ and $+4.78$ cm^{-1} and $g = 2.09$ and 2.05 with an error $R = 8.6 \times 10^{-5}$ and 1.4×10^{-4} for **1** and **2** respectively, where $R = \Sigma[(\chi_m T)_{obs} - (\chi_m T)_{calc}]^2/\Sigma[(\chi_m T)_{obs}]^2$.

The global feature of the $\chi_M T$ *vs.* T curve of complex **3** is characteristic of very weak antiferromagnetic interaction in a tetranuclear nickel(II) complex and/or intermolecular interaction (Fig. 8). The value of $\chi_M T$ at 300 K is 4.6212 cm^3 K mol^{-1} which is slightly high to the expected for four uncoupled nickel(II) ions (4 × 0.99 cm^3 K mol^{-1} with $g = 2.0$). The $\chi_M T$ values are more or less constant at high temperature and then decrease suddenly in the low-temperature region reaching a value of 0.7455 cm^3 K mol^{-1} at 2 K.

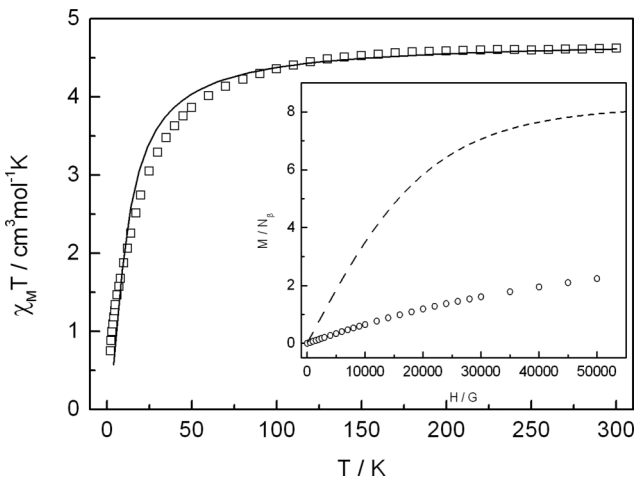

Fig. 8 Plots of the $\chi_M T$ *vs* T and $M\,N^{-1}\beta$ *vs* H at $T = 2$ K (inset) for **3**. Solid and dashed lines correspond to the best fit and the simulation $M\,N^{-1}\beta$ *vs* H at $T = 2$ K with $g = 2$ respectively (see text).

The reduced molar magnetisation ($M\,N^{-1}\beta$) at 2 K for **3** reaches 2.24 (Fig. 8, inset). This value is less than the expected for four isolated Ni(II) ion (8 with $g = 2.0$ Nβ). Confrontation of the overall shape of the plot of the compound with the Brillouin one (dashed plot) for four isolated Ni(II) with $S = 1$ and $g = 2$ at $T = 2$ K indicates slower magnetisation which is consistent with a weak antiferromagnetic interaction.

As in **1** and **2** the structure of **3** consists of nickel ions linked between them by the ligand PyPzOAP giving a tetranuclear compound with the same topology, therefore one coupling parameter J, (Fig. 7) can be considered to interpret the magnetic interactions in the complex using the previous assumption and Hamiltonian of the eqn (1). The analysis of the experimental susceptibility data have been performed by the use of expression (3):

$$\chi_M = \frac{N\beta^2g^2}{kT}\frac{\begin{array}{l}2\exp(J/KT)+14\exp(3J/KT)+22\exp(5J/KT)+52\exp(6J/KT)\\+10\exp(7J/KT)+56\exp(8J/KT)+60\exp(10J/KT)\end{array}}{\begin{array}{l}1+3\exp(J/KT)+11\exp(3J/KT)+\exp(4J/KT)+13\exp(5J/KT)\\+24\exp(6J/KT)+5\exp(7J/KT)+14\exp(8J/KT)+9\exp(10J/KT)\end{array}} \quad (3)$$

The best fit parameters found are: $J = -4.02$ cm^{-1} and $g = 2.17$ with an error $R = \Sigma[(\chi_M T)_{obs}\text{-}(\chi_M T)_{calc}]^2/\Sigma[(\chi_M T)_{obs}]^2 = 6.1 \times 10\text{–}^4$.

The magnetic behavior of **4** in the forms of $\chi_M T$ *vs* T and χ_M *vs* T (inset) plots is shown in Fig. 9. At 300 K, the $\chi_M T$ value per dimer is 0.3203 cm^3 mol^{-1} K, this value is very much smaller than that expected for two uncoupled $S = 1/2$ spins (0.75 cm^3 mol^{-1} K). $\chi_M T$ decreases rapidly with decreasing temperature to reach a plateau at *ca.* 70 K giving a value of 0.00541 cm^3 mol^{-1} K, which indicates the existence of strong antiferromagnetic coupling. The plateau observed at low temperature is may be due to the non coupled Cu(II) ions in the polycrystalline powder sample. The χ_M shows a maximum of 1.07×10^{-3} cm^3 mol^{-1} at 300 K and then decreases, reaching a minimum (7.73×10^{-5} at *ca.* 70 K). The next increase in the χ_M values is indicative of the presence of a small quantity of paramagnetic impurities. The magnetic susceptibility data were quantitatively analyzed by simple treating it as an interacting dimer [eqn (4)].

$$\chi_M = \frac{Ng^2\beta^2}{KT}\left(\frac{2\exp(J/KT)}{1+3\exp(J/KT)}(1-\rho)+\frac{\rho}{2}\right) \quad (4)$$

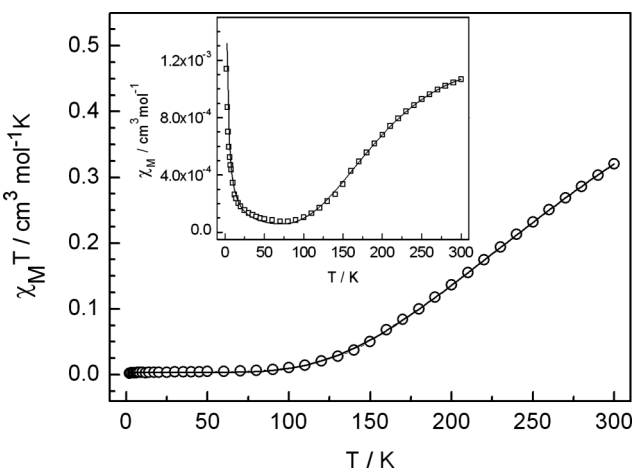

Fig. 9 Plots of $\chi_M T$ *vs.* T and χ_M *vs.* T (inset) for **4**. Solid lines correspond to the best fit (see text).

Here, we take into account a proportion of a monomeric impurity ρ, for which the susceptibility is assumed to follow the

Curie law $\chi = (N\mu_B{}^2 g^2/kT)$. Least-square fitting of all experimental data leads to the following parameters: J = –443.0 cm^{-1}, g = 2.2, and ρ = 0.008 with the agreement factor $R = \sum [(\chi_M)_{obs} - (\chi_M)_{calc}]^2 / \sum[(\chi_M)_{obs}{}^2] = 1.2 \times 10^{-6}$.

EPR spectra of 1

The X-band EPR spectra of **1** at room temperature (Fig. 10) shows an isotropic band centered at $g = 2.11$ (3311 G for $\nu = 9.7920$ GHz) which corresponds to the transition $\Delta M_S = \pm 1$.

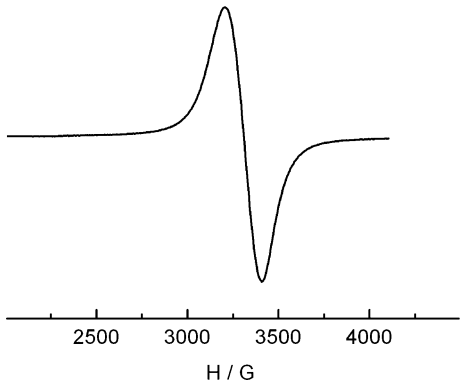

Fig. 10 EPR spectra of **1** at room temperature.

Magnetic interpretation

The values of the superexchange parameters J = +5.88 and +4.78 cm^{-1} for compounds **1** and **2** respectively, are in agreement with the observed ones in the [2 × 2] grid complexes previously reported.[8b,d] These complexes are formed by similar four ligands giving a self-assembled, ferromagnetically coupled tetranuclear Cu^{II} with only one interaction J. The origin of the ferromagnetic coupling can be associated to the quasi orthogonality between copper atoms established recently by theoretical DFT calculations.[8b,d] The pathways interaction, J, is among an apical and equatorial (*a*–*e*) position of the adjacent coppers atoms. Generally, for this kind of interaction one can expect a slight ferro- or anti-ferromagnetic interaction depending on the relative disposition of the planes that contain the magnetic orbitals.[25]

For the antiferromagnetic nickel compound **3** the pathways interaction, J, is also among an apical and equatorial (*a*–*e*) position of the adjacent nickel(II) atoms. In this case, two adjacent orbitals $d_{x^2-y^2}$ and d_{z^2} are located in the same plane causing the propagation of the magnetic exchange *via* the d_{z^2} and $d_{x^2-y^2}$ orbitals which interact with the σ orbitals of the oxygen atoms of the bridging ligand resulting, thus, in a global antiferromagnetic contribution.

For the compound **4**, the significant antiferromagnetic coupling observed is due to the large σ in-plane overlap between the coplanar $d_{x^2-y^2}$ magnetic orbitals and the bridging units. It is well known that the magnitude and nature of the interaction in bis(hydroxo) dinuclear copper(II) complexes depends on several structural parameters such as the Cu–O–Cu angle θ (for $\theta > 97.5°$ coupling is antiferromagnetic and becomes stronger as the θ value increases),[26] Cu–O distances[27] and out-of-plane displacement of the hydrogen atom in the hydroxide group.[28] Considering the established concepts, the Cu–O–Cu angle in **4** is relatively wide (118.4°) obviously falling in the antiferromagnetic regime but not enough to reach a value of J = –443.0 cm^{-1}. The reasons may found in terms of the complementary effect of the HOMO of the second bridging ligand different to the hydroxide.[29,30] Indeed, to transmit the antiferromagnetic coupling, the most useful molecular orbitals of the hydroxide and pyrazolato bridges are the highest filled MOs (HOMOs) which interacts more strongly with the same combination of the atomic $d_{x^2-y^2}$ orbitals allowing more separation between the symmetric φ_s and the antisymmetric φ_a combinations, they add their effect, thus increasing the energy gap $\Delta = E(\varphi_s) - E(\varphi_a)$ and consequently increasing the J_{AF} values as was demonstrated by the theoretical calculations reported by Escriva *et al.*[30] in (μ- hydroxo)(μ-pyrazolato) dicopper(II) model. In view of this, the coupling constant of J = –443.0 cm^{-1} calculated for **4** is in accordance with expectation.

Conclusion

The mixed pyrazole-pyridine based ditopic ligands PyPzOAP and PzOAP self-assemble in the presence of Cu(II) and Ni(II) salts to form a series of [2 × 2] molecular grids. The ligand PyPzOAP forms a Cu_4(II) grid **1** and a Ni_4(II) grid **3** whereas, the ligand PzOAP forms the Cu_4(II) grid **2**. One polytopic ligand 2-PzCAP having a linear arrangement of a number of coordination pockets forms solely a dicopper(II) complex **4**. The ligand negates our expectation for grid formation. This is probably due to the six-membered (not five) chelate rings in the tridentate N3 coordinating pockets of 2-PzCAP ligand. In **1** and **3** all the metal centers have distorted octahedral geometry, whereas in **2**, all the four Cu(II) centers have a square pyramidal geometry. In the dicopper(II) complex **4**, both the metal centers have square pyramidal geometry. The square copper clusters (**1** and **2**) exhibit intramolecular ferromagnetic spin exchange associated with orthogonal alkoxide bridging arrangement and close proximity of the Cu(II) centers. The square Ni(II) complex (**3**) exhibits intramolecular antiferromagnetic exchange in which the four octahedral Ni(II) centers are bridged by alkoxide groups with a Ni–O–Ni bridge angle 137.83 (13)°. There is a fundamental difference between the magnetic behaviours of Cu(II) and Ni(II) grids of the same ligand which is in agreement with previous reports.[14]

Acknowledgements

Financial support [Sanc. No. SR/S1/IC-27/2008, dated 13.03.2009] from Department of Science & Technology (DST), New Delhi, India, is gratefully acknowledged. T.N.M. thanks the University Grants Commission, New Delhi, India, for financial assistance. The Spanish (CTQ2009-07264/BQU) and Catalan (2009 SGR-1454) financial support are acknowledged.

References

1 (*a*) M.-T. Youinou, N. Rahmouni, J. Fischer and J. A. Osborn, *Angew. Chem., Int. Ed. Engl.*, 1992, **31**, 733; (*b*) G. S. Hanan, D. Volkmer, S. S. Ulrich, J.-M. Lehn, G. Baum and D. Fenske, *Angew. Chem., Int. Ed. Engl.*, 1997, **36**, 1842; (*c*) L. Zhao, Z. Xu, L. K. Thompson, S. L. Heath, D. O. Miller and M. Ohba, *Angew. Chem., Int. Ed.*, 2000, **39**, 3114; (*d*) L. N. Dawe, K. V. Shuvaev and L. K. Thompson, *Inorg. Chem.*, 2009, **48**, 3323; (*e*) K. V. Shuvaev, S. S. Tandon, L. N. Dawe and L. K. Thompson, *Chem. Commun.*, 2010, **46**, 4755; (*f*) K. V. Shuvaev, T. S. M. Abedin, C. A. McClary, L. N. Dawe, J. L. Collins and L. K. Thompson,

Dalton Trans., 2009, 2926; (*g*) L. N. Dawe, K. V. Shuvaev and L. K. Thompson, *Chem. Soc. Rev.*, 2009, **38**, 2334; (*h*) Y. S. Moroz, K. Kulon, M. Haukka, E. Gumienna-Kontecka, H. Koztowski, F. Meyer and I. O. Frictsky, *Inorg. Chem.*, 2008, **47**, 5656 and references therein.
2 M. Ruben, J. Rojo, F. J. Romero-Salguero, L. H. Uppadiene and J.-M. Lehn, *Angew. Chem., Int. Ed.*, 2004, **43**, 3644.
3 M. Ruben, J.-M. Lehn and P. Müller, *Chem. Soc. Rev.*, 2006, **35**, 1056.
4 J.-M. Lehn, *Supramolecular Chemistry-Concepts and Perspective*, VCH, Weinheim, 1995.
5 L. K. Thompson, L. Zhao, Z. Xu, D. O. Miller and W. M. Reiff, *Inorg. Chem.*, 2003, **42**, 128 and references therein.
6 (*a*) M. Andruh, *In Encyclopedia of Supramolecular Chemistry*, J. L. Atwood and J. W. Steed, ed., Marcel Dekker, Inc., New York, 2004, pp 1186-1193; (*b*) M. Ruben, E. Breuning, J.-M. Lehn, V. Ksenofontov, F. Renz, P. Gütlich and B. M. Vaughan, *Chem.–Eur. J.*, 2003, **9**, 4422; (*c*) Waldmann, O Waldmann, J. Hassmann, P. Müller, G. S. Hanan, D. Volkmer, U. S. Schubert and J.-M. Lehn, *Phys. Rev. Lett.*, 1997, **78**, 3390.
7 (*a*) J. Rojo, F. J. Romero-Salguero, J.-M. Lehn, G. Baum and D. Fenske, *Eur. J. Inorg. Chem.*, 1999, 1421; (*b*) O. Waldmann, M. Ruben, U. Zeiner and J.-M. Lehn, *Inorg. Chem.*, 2006, **45**, 6535; (*c*) O. Waldmann, J. Hassmann, P. Müller, D. Volkmer, U. S. Schubert and J.-M. Lehn, *Phys. Rev. B: Condens. Matter*, 1998, **58**, 3277; (*d*) V. A. Milway, S. M. T. Abedin, V. Niel, T. L. Nelly, L. N. Dawe, S. K. Dey, D. W. Thompson, D. O. Miller, M. S. Alam, P. Müller and L. K. Thompson, *Dalton Trans.*, 2006, 2835.
8 (*a*) L. N. Dawe and L. K. Thompson, *Angew. Chem., Int. Ed.*, 2007, **46**, 7440; (*b*) S. Roy, T. N. Mandal, A. K. Barik, S. Pal, R. J. Butcher, M. S. E. Fallah, J. Tercero and S. K. Kar, *Dalton Trans.*, 2007, 1229; (*c*) S. Roy, T. N. Mandal, A. K. Barik, S. Gupta, R. J. Butcher, M. S. E. Fallah, J. Tercero and S. K. Kar, *Dalton Trans.*, 2009, 8215; (*d*) S. Roy, T. N. Mandal, A. K. Barik, S. Gupta, R. J. Butcher, M. S. E. Fallah, J. Tercero and S. K. Kar, *Polyhedron*, 2008, **27**, 105.
9 M. J. Grannas, B. F. Hoskins and R. J. Robson, *J. Chem. Soc., Chem. Commun.*, 1990, 1644.
10 M. J. Grannas, B. F. Hoskins and R. Robson, *Inorg. Chem.*, 1994, **33**, 1071.
11 L. H. Uppadeine, J. P. Gisselbrecht, N. Kyritsakas, K. Nättinen, K. Rissamen and J. M. Lehn, *Chem.–Eur. J.*, 2005, **11**, 2549.
12 L. Zhao, C. J. Matthews, L. K. Thompson and S. L. Heath, *Chem. Commun.*, 2000, 265.
13 D. M. Bassani, J. M. Lehn, K. Fromm and D. Fenske, *Angew. Chem., Int. Ed.*, 1998, **37**, 2364.
14 C. J. Matthews, K. Avery, Z. Xu, L. K. Thompson, L. Zhao, D. O. Miller, K. Biradha, K. Poirier, M. J. Zaworotko, C. Wilson, A. E. Goeta and J. A. K. Howard, *Inorg. Chem.*, 1999, **38**, 5266.
15 V. McKee and S. S. Tandon, *J. Chem. Soc., Chem. Commun.*, 1988, 1334.
16 Z. Xu, L. K. Thompson and D. O. Miller, *J. Chem. Soc., Dalton Trans.*, 2002, 2462.
17 D. D. Perrin, W. L. F. Armarigo and D. R. Perrin, *Purification of Laboratory Chemicals, Second edn*, Pergamon Press, Oxford, 1980.
18 T. N. Mandal, S. Roy, A. K. Barik, S. Gupta, R. J. Butcher and S. K. Kar, *Polyhedron*, 2008, **27**, 3267.
19 S. K. Dey, T. S. M. Abedin, L. N. Dawe, S. S. Tandon, J. L. Collins, L. K. Thompson, A. V. Postnikov, M. S. Alam and P. Mü1ller, *Inorg. Chem.*, 2007, **46**, 7767.
20 G. M. Sheldrick, *SHELXS-97 and SHELXL-97*, University of Göttingen, Germany, 1997.
21 A. L. Spek, PLATON, Molecular Geometry Program, *J. Appl. Crystallogr.*, 2003, **36**, 7.
22 L. J. Farrugia, *J. Appl. Crystallogr.*, 1997, **30**, 565.
23 L. J. Farrugia, *J. Appl. Crystallogr.*, 1999, **32**, 837.
24 K. Kambe, *J. Phys. Soc. Jpn.*, 1950, **5**, 48.
25 P. J. Hay, J. C. Thibeault and R. Hoffmann, *J. Am. Chem. Soc.*, 1975, **97**, 4884.
26 V. H. Crawford, H. W. Richardson, J. R. Wasson, D. J. Hodgson and W. E. Hatfield, *Inorg. Chem.*, 1976, **15**, 2107.
27 E. Ruiz, P. Alemany, S. Alvarez and J. Cano, *Inorg. Chem.*, 1997, **36**, 3683.
28 E. Ruiz, P. Alemany, S. Alvarez and J. Cano, *J. Am. Chem. Soc.*, 1997, **119**, 1297.
29 M. S. El Fallah, F. Badyine, R. Vicente, A. Escuer, X. Solans and M. Font-Bardia, *Dalton Trans.*, 2006, 2934 and references therein.
30 E. Escrivà, J. García-Lozano, J. Martínez-Lillo, H. Nuñez, J. Server-Carrió, L. Soto, R. Carrasco and J. Cano, *Inorg. Chem.*, 2003, **42**, 8328.